Electronic Supplementary Material (ESI) for Nanoscale Horizons.

Vertical heterostructure of graphite-MoS_2 for gas sensing

M. Tripathi[1*#], G. Deokar[2#], J. Casanova-Chafer[3], J. Jin[2], A. Sierra-Castillo[4], S. P. Ogilvie[1], F. Lee[1, 5], S. A. Iyengar[6], A. Biswas[6], E. Haye[7], A. Genovese[8], E. Llobet[3], J- F Colomer[4], I. Jurewicz[9], V. V. Gadhamshetty*[10], P.M. Ajayan[6], Udo Schwingenschlögl[2], Pedro M. F. J. Costa[2], A. B. Dalton[1*]

[1] Department of Physics and Astronomy, University of Sussex, Brighton BN1 9RH, U.K.
[2] King Abdullah University of Science and Technology (KAUST), Physical Science and Engineering Division, Thuwal, 23955 - 6900, Saudi Arabia
[3] Universitat Rovira i Virgili, MINOS, Avda. Països Catalans, 26, 43007 Tarragona, Spain
[4] Research Group on Carbon Nanostructures (CARBONNAGe), University of Namur, 5000 Namur, Belgium.
[5] International Institute for Nanocomposites Manufacturing (IINM), WMG, University of Warwick, Coventry CV47AL,U.K.
[6] Department of Materials Science and NanoEngineering, Rice University, Houston, Texas 77005, United States.
[7]Laboratoire d'Analyse par Réactions Nucléaires (LARN), Namur Institute of Structured Matter (NISM), University of Namur, 61 Rue de Bruxelles, 5000 Namur, Belgium
[8] King Abdullah University of Science and Technology, Core Labs, Thuwal, 23955-6900, Saudi Arabia
[9]Department of Physics, Faculty of Engineering & Physical Sciences, University of Surrey, Guildford GU2 7XH, UK
[10]Department Civil and Environmental Engineering, South Dakota School of Mines and Technology, Rapid City, SD, 57701 USA

Supplementary Information

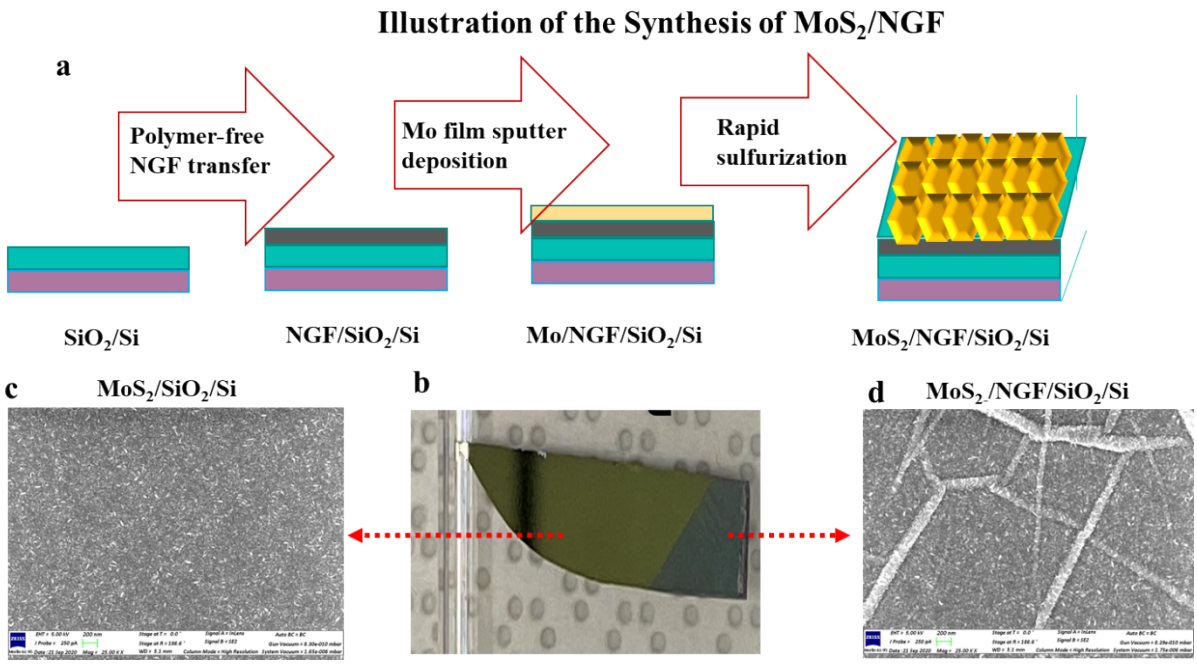

Figure S1: Preparation of the hybrid structure. Schematic view illustrating the different stages of formation of vertically aligned MoS_2 over nano-thick graphite surface. Initially, there is a polymer-free transfer of graphite film (NGF) over the silica substrate, followed by Mo sputtering and rapid sulfurization. (b) The optical image contrast of the MoS_2 sheet over Silica substrate and graphite are marked by arrows for distinction. (c) SEM micrography of MoS_2 granular sheet over silica. (d) SEM micrograph of MoS_2 granular sheet over wrinkled graphite layers.

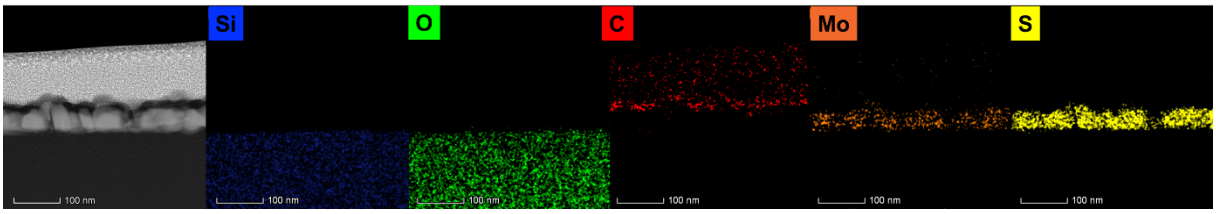

Figure S2: Cross-section view of the hierarchy of the hetero-hybrid structure. Left-hand side is SEM image of hierarchical architecture as (top) $MoS_2/NGF/SiO_2/Si$ substrate. In the series of images from left to right-hand side, there is the elemental distribution in the Z-direction revealing the hierarchy of Si, O, C, Mo, S, respectively. It is worth noting that the elemental mapping of carbon is not from the NGF but a deposited polymeric layer during Energy-

dispersive X-ray (EDX) analysis. The NGF layers sandwiched between SiO_2 and MoS_2 is too thin to resolve in the present setup.

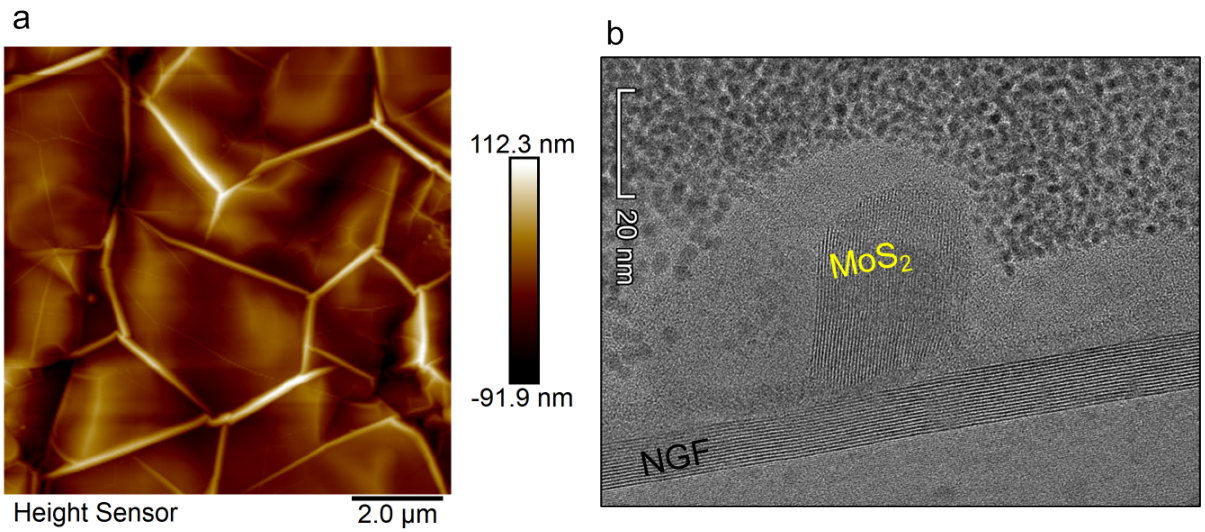

Figure S3: (a) AFM topography of NGF surface shows top-view landscale of graphene wrinkles, grain boundary (depression region) and basal plane. (b) High-resolution side view TEM image of NGF and MoS_2 shows horizontal stacking of graphite sheets and vertically aligned MoS_2.

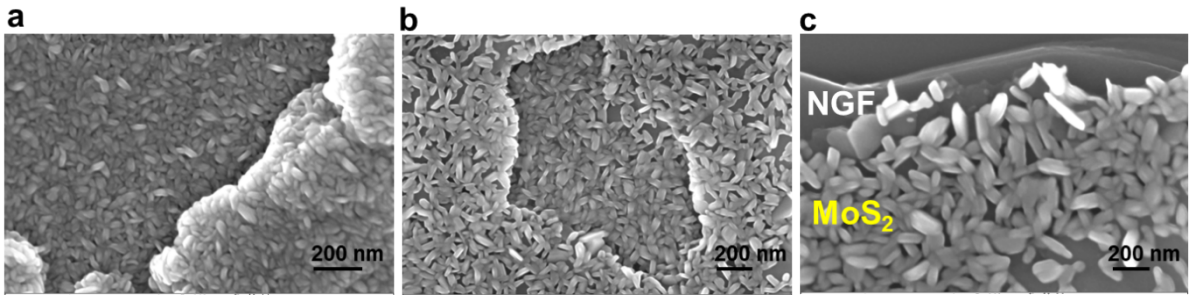

Figure S4: Appearance of the hybrid heterostructure. SEM micrographs of MoS_2 granular flakes distribution over NGF at different locations (a) basal plane, (b) structural defect and (c) step-edge. The density of MoS_2 varies with the size of Mo NPs, the size of 10 nm Mo film is relatively less populated than that of 20 nm Mo sulfurized film.

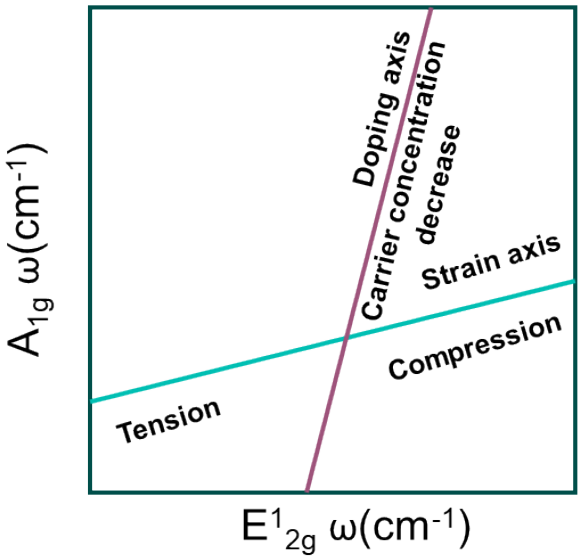

Figure S5: Schematic correlation plot of MoS_2 deconvoluting strain and doping

The Raman peak shifts ω of E^1_{2g} and A_{1g} from the strain-free and doping-free positions can be related to the mechanical strain ε and the electrical doping n by a linear transformation, *i.e.*,

$$\begin{pmatrix} \omega_{E^1_{2g}} \\ \omega_{A_{1g}} \end{pmatrix} = \begin{pmatrix} -2\gamma_{E^1_{2g}} & k_{E^1_{2g}} \\ -2\gamma_{A_{1g}} & k_{A_{1g}} \end{pmatrix} \begin{pmatrix} \varepsilon \\ n \end{pmatrix}$$

where $\gamma_{E^1_{2g}} = 0.86$ and $\gamma_{A_{1g}} = 0.15$ are the Grüneisen parameters, while $k_{E^1_{2g}} = -0.33 \times 10^{-13}\, cm^{-1}$ and $k_{A_{1g}} = -2.22 \times 10^{-13}\, cm^{-1}$ are the doping shift rates. With this linear transformation, the strain and doping axes, as well as iso-strain and iso-doping contours can be constructed. The strain and doping can then be evaluated by projecting the peak positions onto the strain and doping axes.

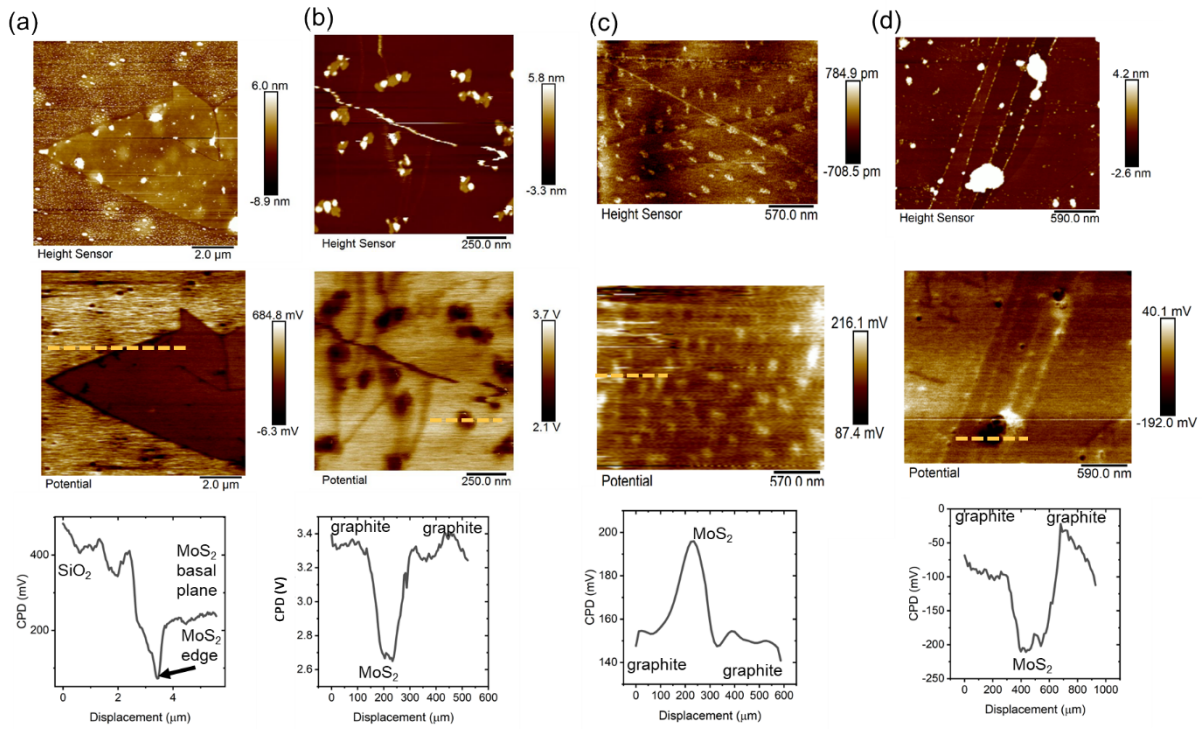

Figure S6: Surface potential map of MoS_2 and vertical heterostructure of MoS_2 over graphite. (a) Surface potential map of an MoS_2 over silica substrate. The surface potential reveals the contrast in contact potential difference (CPD, mV/V), indicating the distribution in carrier concentration. The brightest region represents the p-doped region (silica substrate), and the dark region represents the electron-rich region. Here, the edges of MoS_2 reveal the higher electron concentration, indicating a drop in the CPD values confirmed by the average line profile. (b) The surface potential map of MoS_2 over graphite flakes shows higher electron concentration in MoS_2, indicated through dark colour in the CPD map and a decrease in the surface potential profile. (c) Exposure of the MoS_2-graphite heterostructure to nitronium ions shows p-doping of MoS_2, as indicated by the increase in the CPD values. (d) Exposure of the MoS_2-graphite heterostructure to ammonium ions shows n-type doping in the MoS_2 , as there is the drop in the CPD values.

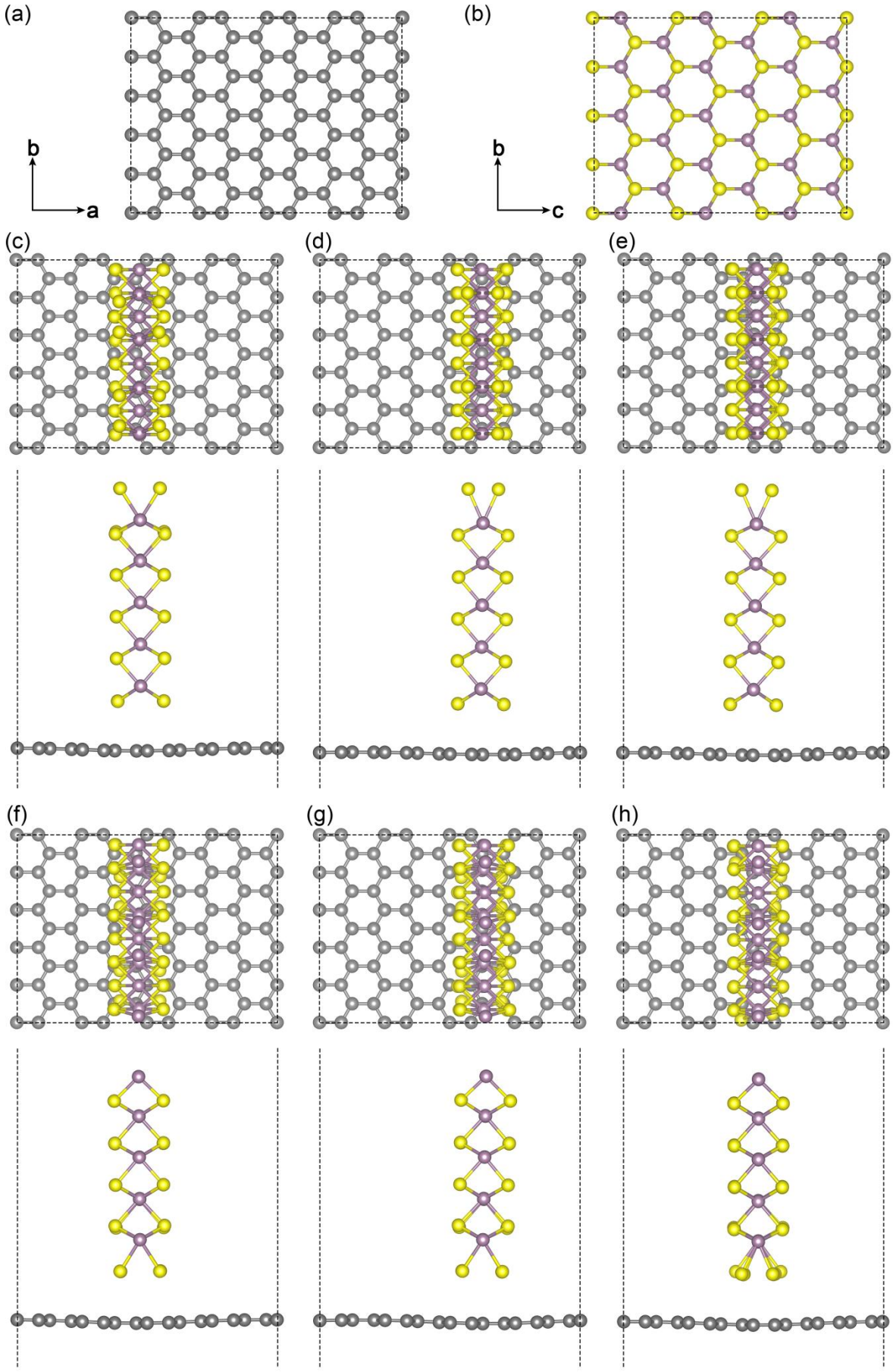
(a)
b
a
(b)
b
c
(c)
(d)
(e)
(f)
(g)
(h)

Figure S7: Density functional theory simulations. (a, b) Top views of the graphene and MoS_2 supercells. Optimized structures of the stacking configurations (c) AB, (d) AB1, and (e) AB2 of the S-terminated MoS_2 on graphene. Optimized structures of the stacking configurations (f) AB, (g) AB1 and (h) AB2 of the Mo-terminated MoS_2 on graphene.

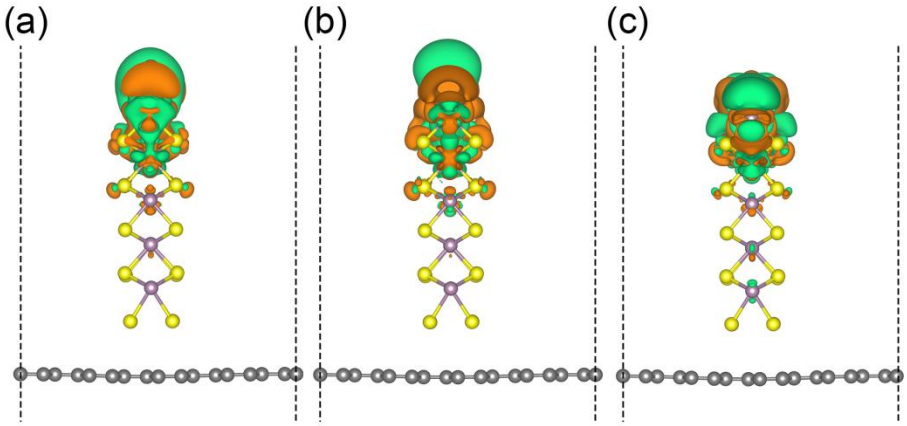

Figure S8: Charge transfer. Side views of the charge redistributions between the graphene/MoS_2 hybrid structure with Mo-termination (towards the analyte molecules) and (c) H_2O, (d) NH_3, and (e) NO_2. Green and orange isosurfaces (isovalue: 0.001 electrons/Å^3) represent charge depletion and accumulation, respectively. The gray, yellow, purple, white, red, and blue spheres represent the C, S, Mo, H, O, and N atoms, respectively.

Table S1: Adsorption energies (E_a) of the analyte molecules and charge transfer (Δq) between the graphene/MoS_2 hybrid structure and analyte molecules. Positive (negative) Δq represents charge transfer from the graphene/MoS_2 hybrid structure to the analyte molecules (from the analyte molecules to the graphene/MoS_2 hybrid structure).

	H_2O		NH_3		NO_2	
	E_a	Δq	E_a	Δq	E_a	Δq
S-termination	-0.09	0.01	-0.11	-0.01	-0.13	0.21
Mo-termination	-1.20	0.10	-1.55	-0.05	-4.42	1.02

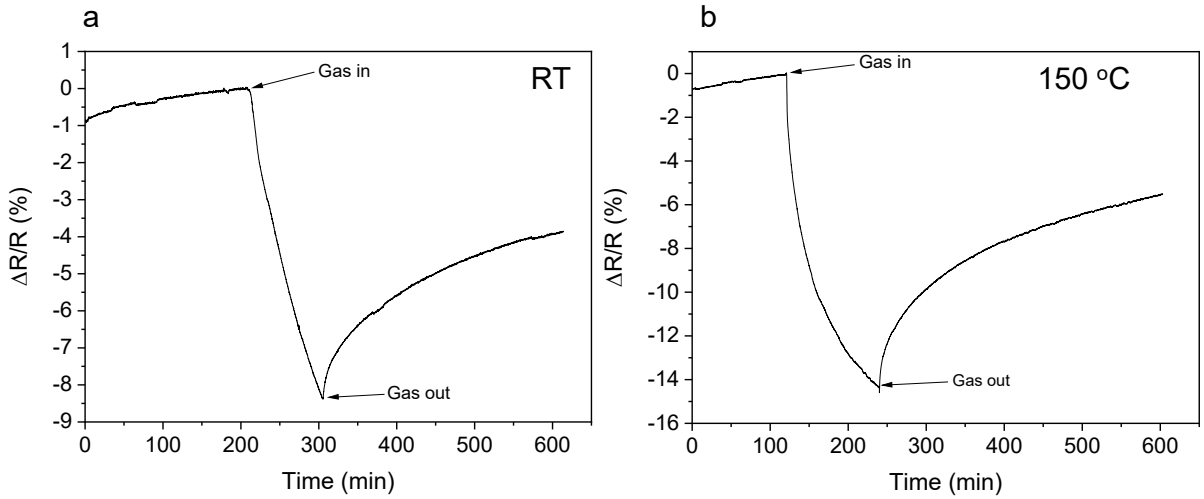

Figure S9: Recovery tests when detecting NO_2, left side (room temperature) and right (150 ºC)

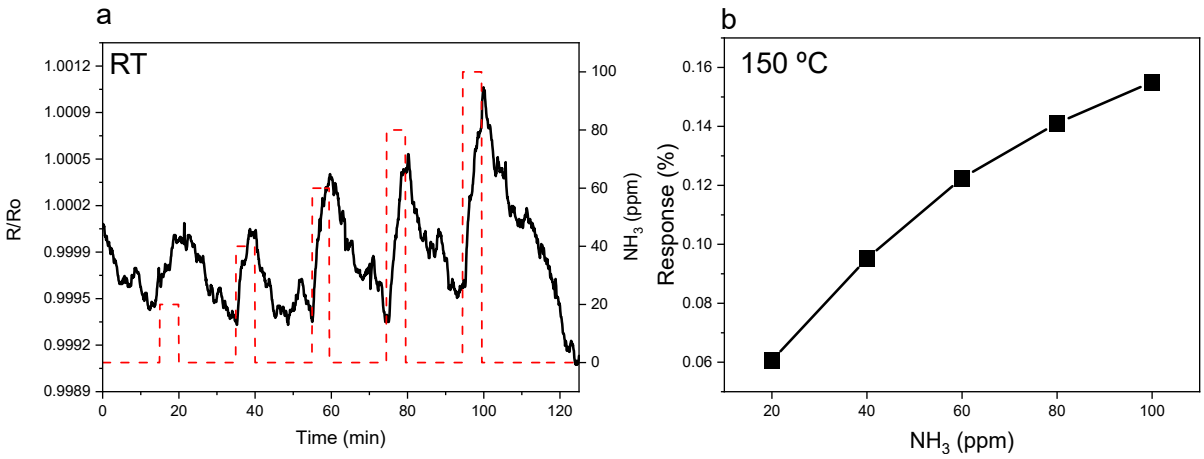

Figure S10: Increment in the response from the hybrid sensor during NH_3 exposure for different concentrations at elevated temperatures.

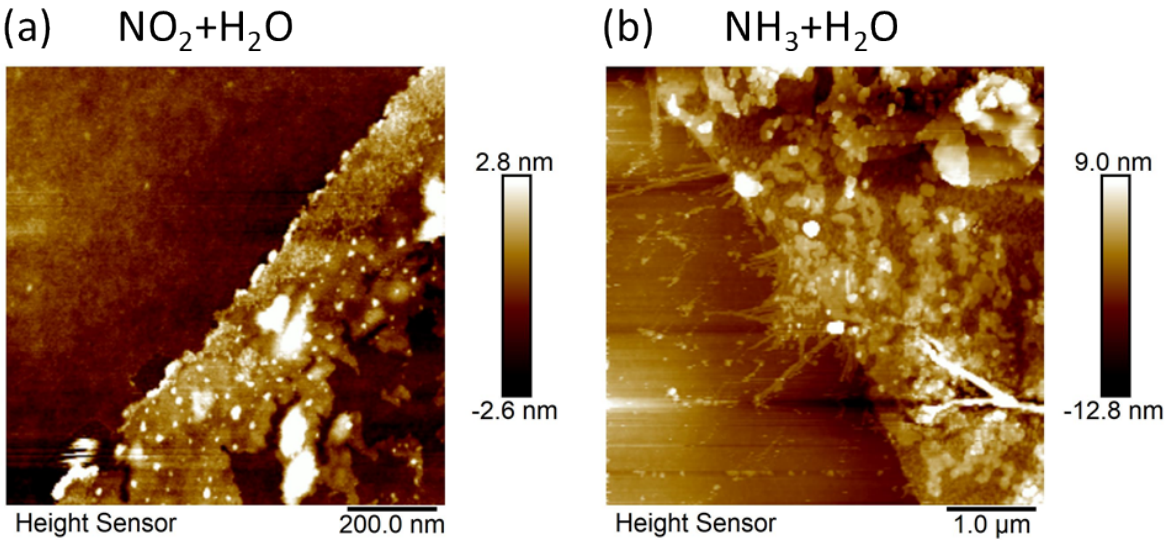

Figure S11: **Morphology of exposed MoS_2**. (a) Topography of MoS_2 treated with (a) aqueous solution of NO_2 and (b) NH_3 as NH_4OH. The topography was taken after drying of the solution and accumulation of salts were monitored. The ammonium salts are distributed uniformly over the basal plane of MoS_2, while salts of the nitro group mostly appear at the edge of MoS_2.

Table S2. Performance comparison in the detection of NO_2 with previously reported sensors.

Nanomaterial	**T° (C)**	**Carrier gas**	**Sensitivity coefficient (response/ppm)**	**RH study**	**Flow rate (sccm)**	**Reference**
MoS_2/Graphite	**150**	**Air**	**1.67**	**Yes**	**100**	**Current work**
UFew-Layer Graphene (FLG)	100	Air	0.83	Yes	100	Deokar et al. [1]
MoS_2/VACNT	RT/100[a]	Air	0.64	Yes	100	Deokar et al.[2]
MoS_2/Graphene	RT (UV)	Air	0.08	No	NA	Kumar et al. [3]
MoS_2/rGO	60	Air	0.02	Yes	500	Zhou et al.[4]
MoS_2-rGO/CNT	RT (UV)	Air	0.017	No	NA	Ghasemi[5]
MoS_2/rGO	RT	Nitrogen	0.004	No	1000	Mukherjee et al.[6]

MoS_2/rGO	50	Air	0.6	No	175	Kumar et al.[7]
MoS_2/GA	200	Air	3.4	No	300	Long et al.[8]
Pure MoS_2	100	Air	1.4	Yes	100	Annanouch et al. [9]

Reference:

1. G. Deokar, J. Casanova-Cháfer, N. S. Rajput, C. Aubry, E. Llobet, M. Jouiad and P. M. F. J. Costa, *Sensors and Actuators B: Chemical*, 2020, **305**, 127458.
2. G. Deokar, P. Vancso, R. Arenal, F. Ravaux, J. Casanova-Cháfer, E. Llobet, A. Makarova, D. Vyalikh, C. Struzzi and P. Lambin, *Advanced Materials Interfaces*, 2017, **4**, 1700801.
3. R. Kumar, N. Goel and M. Kumar, *ACS sensors*, 2017, **2**, 1744-1752.
4. Y. Zhou, G. Liu, X. Zhu and Y. Guo, *Sensors and Actuators B: Chemical*, 2017, **251**, 280-290.
5. F. Ghasemi, *Scientific Reports*, 2020, **10**, 11306.
6. A. Mukherjee, L. R. Jaidev, K. Chatterjee and A. Misra, *Nano express*, 2020, **1**, 010003.
7. R. Kumar, N. Goel, A. V. Agrawal, R. Raliya, S. Rajamani, G. Gupta, P. Biswas, M. Kumar and M. Kumar, *IEEE Sensors Journal*, 2019, **19**, 10214-10220.
8. H. Long, A. Harley-Trochimczyk, T. Pham, Z. Tang, T. Shi, A. Zettl, C. Carraro, M. A. Worsley and R. Maboudian, *Advanced Functional Materials*, 2016, **26**, 5158-5165.
9. F. E. Annanouch, A. Alagh, P. Umek, J. Casanova-Chafer, C. Bittencourt and E. Llobet, *Journal of Materials Chemistry C*, 2022, **10**, 11027-11039.